Check for updates

Toward phosphorescent and delayed fluorescent carbon quantum dots for next-generation electroluminescent displays

Ting Yuan, Ting Meng, Yuxin Shi, Xianzhi Song, Wenjing Xie, Yunchao Li, [ID] Xiaohong Li, [ID] Yang Zhang [ID] * and Louzhen Fan [ID] *

Featuring a combination of size-tunable emission wavelengths, high thermal stability, and low cytotoxicity, carbon quantum dots (CQDs) have opened up a new possibility for next-generation displays. However, the theoretically highest external quantum efficiency (EQE) limit of electroluminescent light-emitting diodes (LEDs) based on fluorescent CQDs is 5% due to the spin-forbidden nature of triplet state transitions. Comparatively, phosphorescent or delayed fluorescence CQDs are expected to overcome this limitation and allow the EQE of the devices to reach nearly 25%. At present, the preparation of CQDs with good solution processability, narrow bandwidth emission, and full-color phosphorescence or delayed fluorescence still faces great challenges. Herein, this review aims to offer a materials-chemistry perspective to tailor highly efficient phosphorescent or delayed fluorescence CQDs and present their applications in electroluminescent LEDs for the display technology. The mechanism and design principle of pure organic phosphorescence and delayed fluorescence as well as their recent advances in electroluminescent devices are summarized. Furthermore, we focus on the prospects and challenges for phosphorescent and delayed fluorescence CQDs in displays. We hope that this review will further stimulate the development of high-performance CQD-based electroluminescent displays with a combined effort from different disciplines.

1. Introduction

The world has entered the modern information age with abundant content. Display instruments have become the most important information carrier in daily life and are used in

College of Chemistry, Key Laboratory of Theoretical & Computational Photochemistry, and Radiopharmaceuticals, Ministry of Education, Beijing Normal University, Beijing, 100875, China. E-mail: y.zhang@bnu.edu.cn, lzfan@bnu.edu.cn

diverse media, including televisions, mobile phones, and other panels. Over the past decades, display technology based on electroluminescent light emitting diodes (LEDs), where electric current is used to directly excite emitters and generate photons leading to potentially higher efficiency in contrast to phosphor-converted LEDs (Fig. 1a and b), has advanced by leaps and bounds toward wide color gamut, high brightness, and long lifetimes.[1–4] Generally, electroluminescent display technologies can be divided into two categories based on the types of

Ting Yuan received her Master's degree in physical chemistry from Beijing Normal University in 2019. She is now a PhD student under the supervision of Prof. Louzhen Fan. Her research interests focus on the synthesis and optoelectronic applications of luminescent carbon nanomaterials.

Ting Yuan

Ting Meng received her Master's degree in physical chemistry from Beijing Normal University in 2019. She is now a PhD student under the supervision of Prof. Louzhen Fan. Her research interests focus on the synthesis and optoelectronic applications of solid-state luminescent carbon nanomaterials.

Ting Meng

luminescent materials, *i.e.*, organic LEDs (OLEDs) and quantum dot LEDs (QLEDs). OLEDs have demonstrated practical applications in flat panel displays for smartphones and televisions after three decades of development.[5–8] So far, however, most OLED products have been fabricated by a vacuum deposition technology that requires high running cost, complicated device structures, and control preciseness, which greatly hinders their further large-area manufacturability.[9–12] In contrast, QLEDs feature solution processability, bright photoluminescence, and narrow bandwidths, making them promising candidates for the fabrication of large-area displays and lightening devices through cost-effective ink-jet printing techniques.[13–16] Giants in the display industry (*e.g.*, Samsung, LG, TCL and BOE) worked together with start-up companies in the QD field (*e.g.*, Nanjing Tech, QD Vision and Nanosys) to produce the so-called QLED television. However, the severe toxic and detrimental effects on humans and the environment are still crucial impediments to the use of Cd^{2+}/Pb^{2+}-based QDs as next-generation displays.[17–19] Thus, it is of great significance to develop an ideal alternative.

Quantum-confined carbon quantum dots (CQDs), which represent a class of zero-dimensional (0D) carbon nanoparticles with sizes below 10 nm, exhibit superior properties to conventional semiconductor QDs, such as environment-friendliness, high stability, and low cost.[20–30] Furthermore, CQDs show tunable bandgaps owing to their quantum confinement effect and high photoluminescence quantum yield (PLQY).[31–36] The emission color of CQDs can be tuned by controlling their size and structure,[37–39] providing access to solution-processable emitters covering ultraviolet, visible and near-infrared wavelength regions (Fig. 1c and d). Immense efforts have been made to develop CQD-based LEDs with intrinsic bandgap emission from deep-blue to near-infrared in the last few years.[25,31,40,41] In particular, unprecedented narrow bandwidth emission was recorded for high color-purity multicolored LEDs,[41] which opens up great prospects of CQDs for the next-generation display technology. It is well known that exciton formation under electrical excitation typically results in 25% singlet excitons and 75% triplet excitons. Unfortunately, 75% of the electrically generated energy is dissipated as heat by triplet excitons in fluorescent CQDs, leading to the theoretically highest external quantum efficiency (EQE) of 5% after considering a light outcoupling efficiency of ∼20% in the device. Therefore, to increase the efficiency of CQD-based electroluminescent devices,

Yuxin Shi received her Master's degree in physical chemistry from Beijing Normal University in 2021. She is now a PhD student under the supervision of Prof. Louzhen Fan. Her research interests are centered on the synthesis and optoelectronic application of fluorescent and phosphorescent carbon nanomaterials.

Yuxin Shi

Xianzhi Song received his Bachelor's degree from Beijing Technology and Business University in 2019. He is now a Master's student under the supervision of Prof. Louzhen Fan. His research interests are in the synthesis and application of fluorescent carbon nanomaterials.

Xianzhi Song

Yang Zhang received his PhD in 2013 under the supervision of Prof. Lothar Dunsch from the Leibniz Institute for Solid State and Materials Research Dresden (IFW Dresden, Germany). In 2014, he joined the Beijing Institute of Nanoenergy and Nanosystems, Chinese Academy of Sciences. In 2019, he joined the College of Chemistry, Beijing Normal University. His research interests focus on nanomaterials and nanodevices for energy conversion and biomedical applications.

Yang Zhang

Louzhen Fan is now a chemistry professor in the College of Chemistry, Beijing Normal University. She received her PhD in physical chemistry in 1998 under the supervision of Prof. Daoben Zhu and Prof. Yongfang Li from the Institute of Chemistry, Chinese Academy of Sciences, Beijing. Her research interests are focused on the synthesis of novel carbon and metal nanomaterials and their applications in biology and energy.
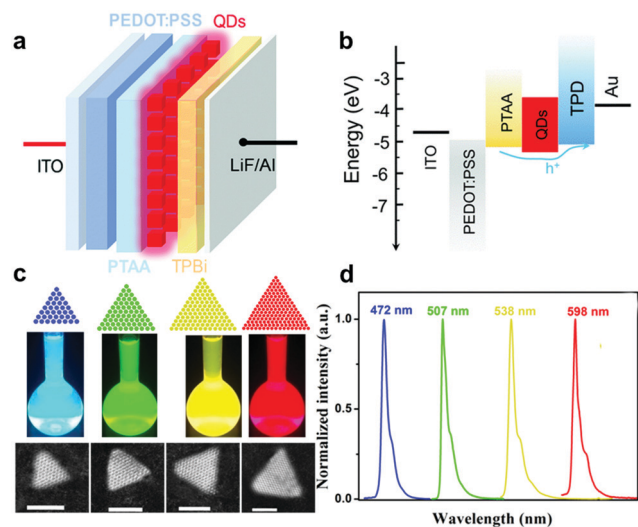
Louzhen Fan

2334 | *J. Mater. Chem. C*, 2022, **10**, 2333–2348

This journal is © The Royal Society of Chemistry 2022

Fig. 1 Device designs and materials for efficient QLEDs in displays. (a) Device structure and (b) energy diagram of QLEDs. Reprinted with permission from ref. 4. Copyright 2019 The Royal Society of Chemistry. (c) Multicolor fluorescent CQDs with size dependence from blue to red and (d) the corresponding PL spectra. Reprinted with permission from ref. 41. Copyright 2018 Springer.

one effective tactic is to break through the theoretical upper limit of quantum efficiency and utilize the non-emissive triplet excitons as much as possible.

The photophysical radiative emission processes of organic excited molecules after light absorption, including not only the traditional fluorescence, but also phosphorescence and thermally activated delayed fluorescence (TADF) due to their complicated excited state electronic structures.[42–44] The latter two phenomena of delayed luminescence correspond to the radiative decay of an excited triplet state or singlet state *via* reverse intersystem crossing (RISC) processes. Accordingly, these two approaches harvest light from both triplet and singlet excitons, allowing the internal quantum efficiency (IQE) of the devices to reach nearly 100%.[45,46] In the last several years, through versatile design principles, such as halogen bonding,[47–49] H-aggregation,[50] and n–π transitions,[51,52] while phosphorescence enhancement strategies based on co-crystallization[49] and rigid matrix host–guest systems,[53–55] pure organic molecules have been progressively endowed with long-lived and strong room-temperature phosphorescence (RTP). Generally, pure organic RTP emitters, including sulfur–nitrogen-containing heteroaromatic derivatives,[56] borate derivatives,[57] polyacid derivatives,[58] *etc.*, are desirable due to the versatility in their molecular design and engineering. However, they often rely on ordered crystal engineering to prevent molecular vibrations and nonradiative deactivation,[59–61] the required critical growth conditions of which inevitably lead to difficulties in preparing high-quality and reliable films for optoelectronic devices. Comparatively, recently CQDs have been extensively investigated with considerable efforts to explore RTP properties for their enormous potential in electroluminescence by taking advantage of their abundant energy level structures.[23,62] The prospect of phosphorescent CQDs has

flourished for several years since the pioneering work by dispersing CQDs into a polyvinyl alcohol matrix in 2013.[63] Then, CQDs with intrinsic RTP properties without the need for additional matrix compositing have also been demonstrated, indicating their potential for ISC and thus showing a new possibility for achieving CQD-based RTP optoelectronic applications.[64–66]

This review primarily aims to provide an illustrative account on recent progress of the mechanism and design of pure organic RTP and TADF emitters as well as their recent advances in electroluminescence to realize next-generation displays. The basic theories and fundamental properties of RTP and TADF of organic materials have been well described in a number of comprehensive reviews.[8,67–74] Herein, we particularly focus on the current challenges and future prospects for RTP and TADF CQDs in displays. Finally, we hope that this review will further stimulate the development of high-performance CQD-based electroluminescent displays with a combined effort from different disciplines.

2. Mechanism of pure organic RTP and TADF

2.1 Basic concepts of pure organic RTP and TADF

As compared to inorganic luminescence, light emission from organic counterparts is much more complicated due to their rich and highly flexible excited state structures, resulting in diverse luminescent phenomena, such as fluorescence, phosphorescence, TADF, *etc.*, which depends on the multiple spin state during the radiative relaxation process. Fluorescence refers to the emission of light between energy states of the same spin multiplicity (from singlet excited states S_1 to ground states S_0) within nanoseconds, while phosphorescence is the emission of light between states with different spin multiplicities (from triplet excited states T_1 to S_0) with lifetimes in the microsecond to second regime. In addition, when T_1 and S_1 are close in energy, the singlet–triplet energy splitting (ΔE_{ST}) is small, and the endothermic RISC process can be overcome by the thermal motions of the molecular atoms. As a result, the nonradiative triplet excitons, due to a spin-forbidden $T_1 \rightarrow S_0$ transition, are transformed to singlet excitons *via* RISC, leading to TADF emission ($S_1 \rightarrow S_0$) with lifetimes in the range of hundreds of nanoseconds to dozens of milliseconds (Fig. 2). In general, EQE is one of the most essential parameters for evaluating the performance of electroluminescent LEDs, which is defined as the ratio of the number of emitted photons outside the device to the number of charges injected into the device. However, only the radiative transition process of singlet excitons from S_1 to S_0 can be utilized for emitting light, *i.e.*, fluorescence, which is quantum-mechanically allowed. Therefore, in organic fluorescent materials, the electrically generated 75% triplet excitons are emitted as heat rather than light. Even if the PLQY of conventional fluorescent molecules can reach nearly 100%, in theory, the EQE maximum (EQE_{max}) value may only reach roughly 5% due to the light out-coupling efficiency of ~20%

This journal is © The Royal Society of Chemistry 2022

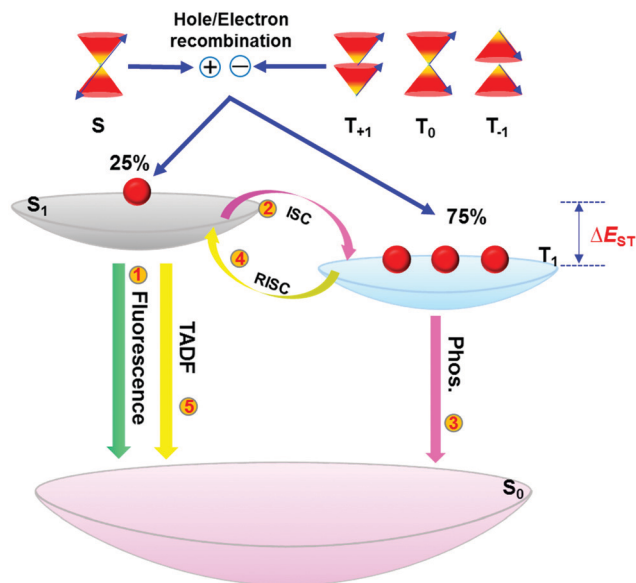*J. Mater. Chem. C*, 2022, **10**, 2333–2348 | **2335**

Fig. 2 Electroluminescence processes in phosphorescent and TADF materials. The transition process of electrically generated excitons for fluorescence (①), phosphorescence (②–③) and TADF (④–⑤). ①: Fluorescence, ②: intersystem crossing (ISC), ③: phosphorescence, ④: reversible intersystem crossing (RISC).

in the electroluminescent device. In contrast, the phosphorescent and TADF emitter capable of harvesting light from both triplet and singlet excitons allow a great break-through of the exciton statistical limit in fluorescent counterparts from 25% to 100% (Fig. 2), which is critically required for the enhanced efficiency. For instance, the theoretical EQE_{max} of the TADF devices can be estimated using eqn (1):

$$
\begin{aligned}
EQE &= \eta_{int}\eta_{out} = \gamma\eta_r\eta_{PL}\eta_{out} \\
&= \gamma\left[\sum_{k=0}^{\infty}\left(0.75\Phi_{PF}\Phi_{RISC}(\Phi_{ISC}\Phi_{RISC})^k\right.\right. \\
&\quad\left.\left. + 0.25\Phi_{PF}(\Phi_{ISC}\Phi_{RISC}))\right]\eta_{out}\right. \\
&= \gamma\left[0.25\Phi_{PF} + \frac{0.75 + 0.25(1-\Phi_{PF})}{1-\Phi_{PF}}\Phi_{DF}\right]\eta_{out} \\
&= \gamma\left[0.25(\Phi_{PF}+\Phi_{DF}) + 0.75\frac{\Phi_{DF}}{1-\Phi_{PF}}\right]\eta_{out} \\
&= \gamma\left[0.25\eta_{PL} + 0.75\frac{\Phi_{DF}}{1-(\eta_{PL}-\Phi_{DF})}\right]\eta_{out}
\end{aligned}
\tag{1}
$$

where η_{int} is the IQE; η_{out} is the outcoupling constant; γ is the charge balance of injected holes and electrons (ideally $\gamma = 1$); η_γ is the excitation–production singlet-to-triplet ratio; η_{PL} is the photoluminescence efficiency; ϕ_{PF} is the photoluminescence quantum yield of the prompt component; and ϕ_{DF} is the photoluminescence quantum yield of the delayed component. If $\phi_{PF} + \phi_{DF} = \eta_{PL} = 1$, then the IQE can be 100% according to eqn (1). In addition, it should be noted that a high degree of orientation of the transition dipole moment of emitters will effectively increase the η_{out}, leading to a high EQE of the device.[8]

2.2 Factors affecting pure organic RTP

Notably, high quantum efficiencies and short lifetimes (dozens of microseconds) are a prerequisite to realize efficient RTP or TADF emitters for high-performance electroluminescent devices. Promoting ISC to generate triplet excitons and suppress its nonradiative decay is key to achieving enhanced phosphorescence emission. Specifically, according to the first-order perturbation theory and Marcus semiclassical approach in the room-temperature region, the rate constant k_{ISC} of ISC can be expressed using eqn (2):[73]

$$
k_{ISC} = \frac{2\pi}{\hbar}|\langle S|\hat{H}_{SOC}|T\rangle|^2\sqrt{\frac{\pi}{\lambda k_B T}}\exp\left[-\frac{(\Delta E_{ST}-\lambda)^2}{4\lambda k_B T}\right]
\tag{2}
$$

where $\langle S|\hat{H}_{SOC}|T\rangle$ is the SOC matrix element between S_1 and T_1, $\hbar$ is the reduced Planck constant, λ is the total reorganization energy, k_B is the Boltzmann constant, and ΔE_{ST} is the energy gap between the singlet and triplet states. This expression indicates that a large SOC and a small ΔE_{ST} will lead to a high k_{ISC}. Heavy atoms such as Br and I can enhance SOC to increase k_{ISC}. For example, it is found that directed halogen bonding in a co-crystal can activate efficient ISC to realize materials with bright RTP and quantum yields of up to 55%.[49] Furthermore, SOC between S_1 and T_1 is favored when they have different electronic configurations such as $^1n\pi^\star$ and $^3\pi\pi^\star$ or $^1\pi\pi^\star$ and $^3n\pi^\star$, respectively, according to El-Sayed's rule (Fig. 3),[51,67,68] and hence the proportions of hybrid (n, $\pi^\star$) and (π, $\pi^\star$) configurations can be tuned to facilitate a strong SOC for promoting the ISC.[52]

Consequently, incorporating a carbonyl group or heteroatoms (N, S, and P) with lone pair electrons into organic emitters can generate an $n\pi^\star$ transition to enhance SOC. For example, Chi and coworkers proposed that the intermolecular electronic coupling of n and π units in a crystal can promote ISC to achieve persistent RTP with a lifetime of 0.49 s.[51] An excited state with hybrid configurations of $\pi\pi^\star$ and $n\pi^\star$ in appreciable proportions is desired to achieve a balanced lifetime (up to 0.23 s) and efficiency (up to 36.0%).[69] According to
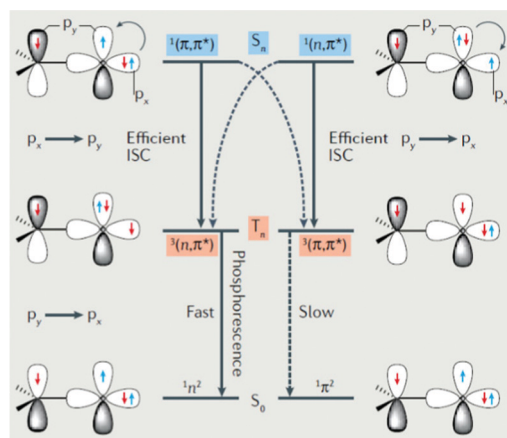

Fig. 3 Schematic illustration of El-Sayed's rule for ISC and its utilization for controlling the phosphorescence decay rate based on the molecular-orbital hybridization of the lowest triplet states. Reprinted with permission from ref. 69. Copyright 2016 Cell Press.

2336 | *J. Mater. Chem. C*, 2022, **10**, 2333–2348

This journal is © The Royal Society of Chemistry 2022

eqn (1), an alternative way to considerably strengthen ISC is to reduce ΔE_{ST}, which has been applied successfully in designing TADF emitters.[8] A design principle based on the realization of small ΔE_{ST} via structural isomerism was used to obtain efficient and ultralong pure organic phosphorescence with a quantum yield of 2.1%.[75]

2.3 Factors affecting TADF

The key process in efficient TADF emitters is the facilitated RISC (T$_1$ → S$_1$), and the dependence of the rate constant of RISC (k_{RISC}) can be expressed as a Boltzmann distribution relation (3):

$$k_{RISC} \propto \exp\left(\frac{\Delta E_{ST}}{k_B T}\right) \qquad (3)$$

where k_B is the Boltzmann constant, T is the temperature, and ΔE_{ST} is the singlet–triplet energy splitting; a small ΔE_{ST} is particularly important according to eqn (3). In principle, ΔE_{ST} is equal to twice the exchange energy J as presented in the following eqn (4):

$$\Delta E_{ST} = E_S - E_T = 2J \qquad (4)$$

In eqn (4), E_S and E_T are the energies of S$_1$ and T$_1$, respectively. For a typical emitter, the two electrons of S$_1$ and T$_1$ states are mainly distributed on the highest occupied molecular orbital (HOMO) and the lowest unoccupied molecular orbital (LUMO), respectively, and the exchange energy J of these two electrons at the HOMO and LUMO can be calculated by the overlap integral of their wave functions as presented in eqn (5):[76]

$$J = \iint \phi_{HOMO}(r_1) \phi_{LUMO}(r_2) \frac{1}{|r_2 - r_1|} \phi_{HOMO}(r_2) \phi_{LUMO}(r_1) dr_1 dr_2$$

$$(5)$$

where ϕ_{HOMO} and ϕ_{LUMO} represent HOMO and LUMO wave functions, respectively. As clearly demonstrated in eqn (5), a small ΔE_{ST} can be realized by minimizing the overlap between the HOMO and LUMO, i.e., spatial wave function separation of the HOMO and LUMO.[77] Therefore, the design of TADF emitters involves spatial separation of the electron-rich (donor) and electron-deficient (acceptor) moieties to separate the HOMO and LUMO distributions and create a small ΔE_{ST} between the S$_1$ and T$_1$ states (Fig. 4a). Several molecular design methods have been presented, including physical separation of donor and acceptor units,[77–79] X-shaped molecular structures,[80] and dual acceptor/donor units.[44] In addition, notably efficient TADF emitters based on the multiple resonance (MR) effect of boron and nitrogen/oxygen atoms have been designed, in which the HOMO and LUMO are separated onto different atoms without the need for electron-rich or electron-deficient substituents (Fig. 4b).[81]

3. Design of pure organic RTP and TADF emitters

Continuous efforts have been devoted to formulating rational rules for designing bright pure organic RTP and TADF in recent years. In general, a unique class of organic RTP emitters can be designed systematically through major strategies based on halogen bonding,[47–49] H-aggregation,[50] and n–π transitions,[51,52] aiming at strengthening the ISC transitions from S$_1$ to T$_1$ and simultaneously depressing the unfavourable non-radiative relaxations of T$_1$ states. As mentioned above, a small ΔE_{ST} to aid the RISC from T$_1$ to S$_1$ is critically required for designing an efficient TADF emitter.

3.1 Design of pure organic RTP emitters

One of the earliest attempts in realizing pure organic phosphorescence relied on the crystallization-induced restriction of intramolecular motions, which can be categorized into pure organic single crystals,[82] ionic crystals,[48] co-crystals[49] and self-assembled crystals[68] based on their packing modes. Furthermore, they are mainly connected by intermolecular interactions, including hydrogen bonding, halogen bonding, ionic bonding, CH–π interactions and π–π interactions. For example, a facile strategy of heavy atom-participated anion–π$^+$ interactions is proposed to construct RTP-active organic salt compounds (1,2,3,4-tetraphenyloxazoliums with different counterions), and the film of TPO-Br exhibited white light emission by simply tuning the degree of crystallization (Fig. 5a–c).[48] Another increasingly explored strategy to design organic RTP with a long lifetime is the stabilization of triplet excitons through molecular H-aggregation,[50] which can be achieved by controlling the
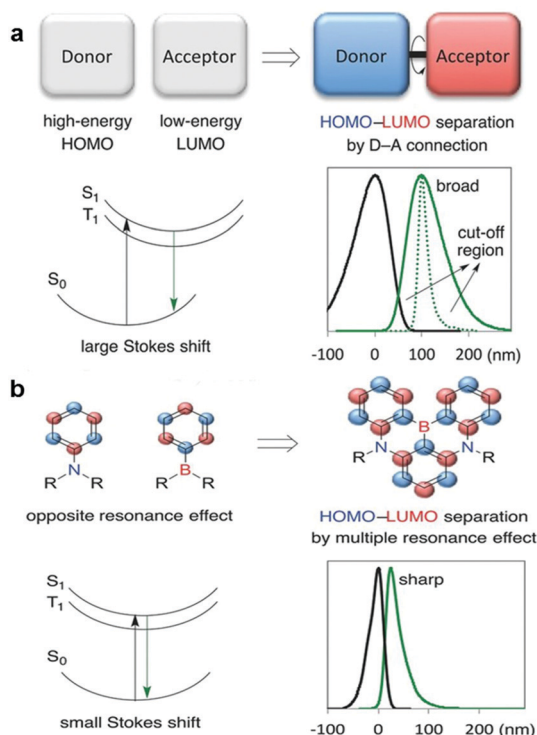

Fig. 4 (a) Conventional design and (b) new design for efficient HOMO–LUMO separation. The localized HOMO and LUMO are indicated by the blue and red colors, respectively. Typical absorption and emission spectra are indicated by the black and green lines, respectively. The blue emission spectrum of a commercial OLED display is indicated by the green dotted line. Reprinted with permission from ref. 95. Copyright 2016 John Wiley and Sons.
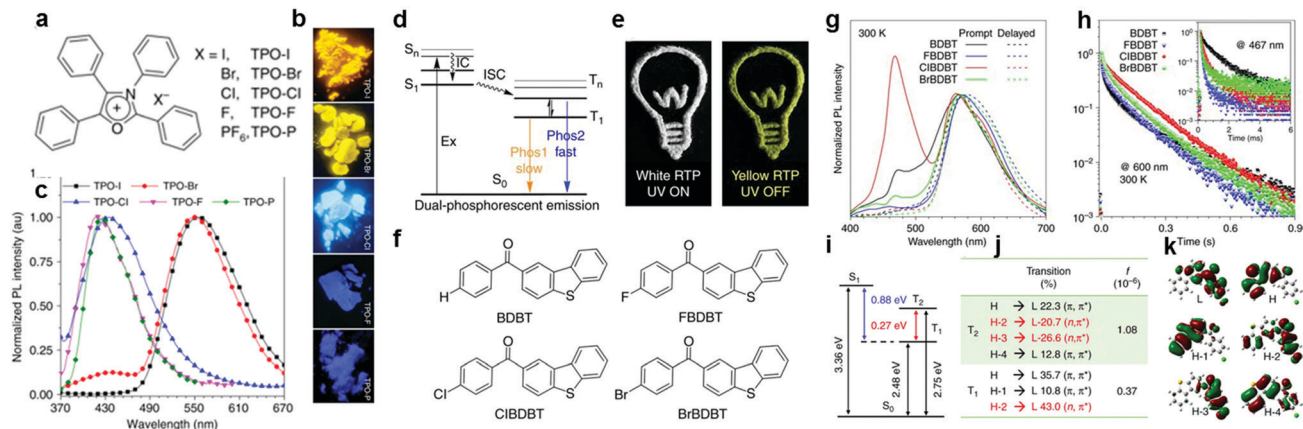
Fig. 5 (a) Chemical structures of TPO-I, TPO-Br, TPO-Cl, TPO-F, and TPO-P. (b) Luminescent photographs and (c) PL spectra of TPO-I, TPO-Br, TPO-Cl, TPO-F, and TPO-P in the solid state. Reprinted with permission from ref. 48. Copyright 2018 Springer. (d) Jablonski diagram for dual phosphorescent emission. (e) Photo-pattern of ClBDBT. (f) Molecular structures of the room temperature phosphors studied here. (g) The prompt (solid line) and delayed (dashed line, 10 ms) PL spectra of the four crystalline powders at 300 K. (h) PL decay curves of 1–4 measured at 600 nm for persistent emission and at 467 nm for fast emission (inset) at 300 K. (i) Calculated adiabatic energy levels, (j) electronic transition characters, and (k) the involved frontier molecular orbitals. Reprinted with permission from ref. 52. Copyright 2017 Springer.

intermolecular interactions in the crystalline state or constructing a small energy gap of $\Delta E_{ST} < 0.3$ eV due to the existence of an energy trapping state T_1^* in organic luminophores. A series of single-component organic crystals featuring colour-tunable ultra-long phosphorescence with lifetime and phosphorescence quantum efficiency of up to 2.45 s and 31.2%, respectively.[59] Another major strategy to promote singlet–triplet ISC in order to produce triplet states and achieve long-lived organic RTP is the enhancement of SOC based on n–π transitions (Fig. 5d–k).[51,52] Specifically, the inclusion of a heavy halogen atom (*i.e.*, Br, Cl, or F), a carbonyl group, and a π-extended dibenzothiophene subunit, *etc.*, is also beneficial in triggering SOC to strengthen the rate of ISC from S_1 to T_n, as well as the rate of radiative relaxation from T_1 to S_0.[46] Furthermore, by varying the π-conjugated units, the (n, π^*) and (π, π^*) molecular orbitals could be mixed to generate tunable T_1 state with distinct $^3(\pi, \pi^*)$ configuration and energy levels, which in turn enabled the tuning of phosphorescence colour and quantum yield.[51] Additionally, apart from achieving efficient ISC, the other key factor for enhancing ϕ_P is suppressing the non-radiative deactivation pathways and reducing the quenching of T_1. These mainly include co-crystal assembly,[49] rigid matrix host–guest systems,[83] structurally modified host–guest systems,[84] and dopant-based systems.[54] By dissolving 1,8-naphthalic anhydride in certain organic solid hosts, purely organic phosphorescence with a lifetime of over 600 ms and an overall quantum yield of over 20% were realized,[55] where it was proposed that a cluster exciton spanning the host and guest forms as a transient state before the guest acts as an energy trap for the RTP state. Overall, the key to achieving efficient phosphorescence lies in enhancing k_{ISC}, accelerating phosphorescent decay and minimizing the non-radiative decay rate and quenching rate. By satisfying these three crucial requirements, the efficiency of pure organic systems exhibiting RTP can be maximized through rational molecular-design principles and aggregation-modulation strategies.

3.2 Design of TADF emitters

Compared to RTP emitters, studies about the design of TADF counterparts are relatively extensive. A small ΔE_{ST} is the dominant driving force for RISC and can be realized through the electron-donating and electron-accepting interactions from intramolecular or intermolecular charge transfer, greatly reducing the overlap of the HOMO and LUMO of the molecules. Various rational design strategies, such as the introduction of a large steric hindrance structure[78,79] or a donor–acceptor system with twist/spiro/bulky connection reducing the overlap between the HOMO and LUMO to enhance the charge transfer state,[80,85] have thus been geared towards generating efficient TADF emission. Despite the significant improvement in EL efficiency, however, the enhanced structural relaxation in the excited states results in broad emission (FWHM of 80–100 nm) with a large Stokes shift in TADF emitters. Thus, to achieve narrowband emission, the HOMO and LUMO can be significantly separated without the need for electron-rich or electron-deficient substituents for a small ΔE_{ST} *via* the MR effect. The strategic introduction of electron-withdrawing imine and electron-donating amine moieties into a versatile boron-embedded 1,3-bis(carbazol-9-yl)benzene skeleton, enabling the systematic hypsochromic and bathochromic shifts of narrowband emissions, respectively, has been demonstrated, achieving a wide visible range from deep blue to yellow (461–571 nm) (Fig. 6).[86]

4. Application of pure organic RTP and TADF emitters in electroluminescent displays

Electroluminescence (EL) based on pure organic RTP and TADF emitters provides an attractive route to harness the non-emissive triplet excitons for display applications.
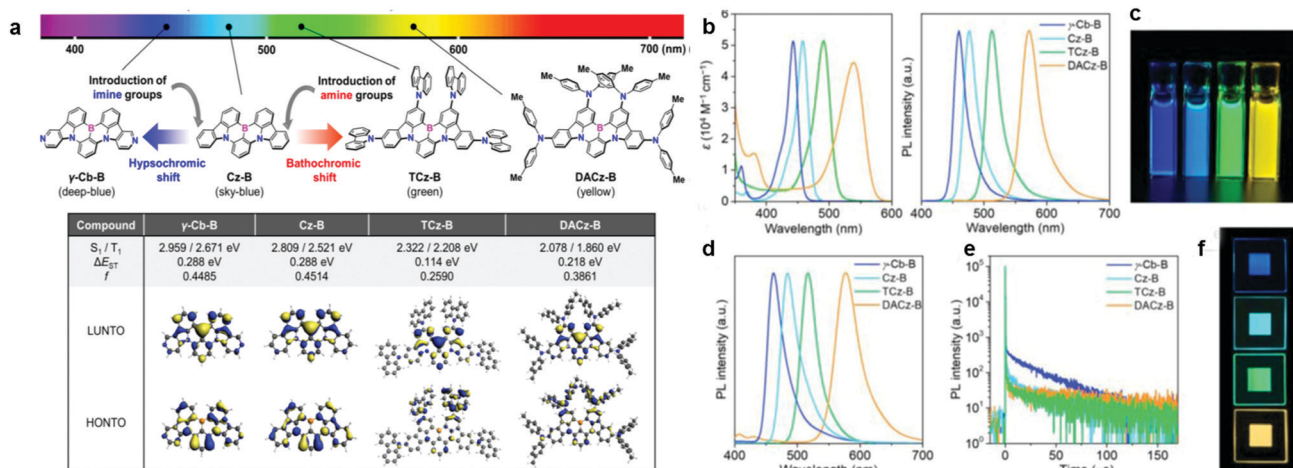
2338 | *J. Mater. Chem. C*, 2022, **10**, 2333–2348

This journal is © The Royal Society of Chemistry 2022

Fig. 6 (a) (top) Design strategy for modulating emission colors in the Cz–B-based MR–TADF systems. (bottom) Summary of theoretical S_1 and T_1 vertical excitation energies, ΔE_{ST} values, oscillator strengths (f), and the associated natural transition orbitals (NTOs). (b) UV–vis absorption (left) and PL (right) spectra of four MR–TADF emitters in deoxygenated toluene solutions (10^{-5} M). (c) Photograph displaying deep-blue to yellow emissions from the solutions under UV illumination at 365 nm. (d) Steady-state PL spectra and (e) transient PL decay curves for the doped films of four MR–TADF emitters. (f) PL images of the doped films vacuum-deposited on quartz substrates. Reprinted with permission from ref. 86. Copyright 2021 John Wiley and Sons.

4.1 Pure organic RTP LEDs

Despite the great potential for display applications, the dependence of ISC and phosphorescence efficiency on efficient SOC as well as the prominent effect of oxygen quenching on the triplet excited state in organic molecules has rendered the realization of pure organic RTP extremely challenging.[48,68,82] Additionally, the lifetimes of pure organic phosphorescent emitters are too long (usually at the millisecond level),[47–56] which will inevitably result in a severe efficiency roll-off at high current densities in electroluminescence due to triplet–triplet exciton annihilation or triplet–polaron annihilation, and thus the applications of pure organic RTP are greatly limited to anti-counterfeiting, optical recording, sensors, biochemistry and security systems.[67,68] Therefore, pure organic phosphorescence that does not require harsh growth conditions with short lifetimes (dozens of microseconds) is required to realize high performance electroluminescent devices, except high phosphorescence quantum efficiencies. Pure organic RTP-based electroluminescent LEDs were firstly demonstrated by Adachi et al. by depositing an organic phosphorescence emitter (compound G5) into a semi-conductive matrix (compound H3) serving as a host to minimize the non-radiative decay of the organic afterglow guest emitters and to act as electron and hole transporters simultaneously.[87] Consequently, the organic phosphorescence can be excited electronically via hole and electron injection and combination in a device structure of indium tin oxide (ITO)/4,4′-bis[N-(1-naphthyl)-N-phenyl-amino] biphenyl (α-NPD) (30 nm)/1,3-bis(N-carbazolyl)benzene (mCP) (10 nm)/1% G5:H3 (30 nm)/1,3,5-tris(N-phenylbenzimidazol-2-yl)benzene (TPBi) (60 nm)/LiF (0.8 nm)/Al (80 nm). The device showed blue fluorescence under an applied voltage and green organic phosphorescence once the applied voltage was turned off, and the lifetime was 0.39 s. Remarkably, an electroactive RTP polymer named P(DMPAc-O-TPTrz) (Fig. 7) has been demonstrated based on a characteristic donor-oxygen-acceptor geometry,

where an oxygen atom (O) is inserted as the spacer between the acridine donor (D) and triazine acceptor (A). The corresponding polymer LEDs reveal a dominant electrophosphorescence with a record-high EQE of 9.7%,[88] which is far higher than the 5% theoretical limit for typical fluorescent emitters, promoting the development of pure organic RTP towards efficient LEDs.

4.2 TADF LEDs

The first attempt to apply TADF materials in OLEDs was made in 2009.[89] The device required a rather high onset of current injection around 10 V and 29 V for 100 mA cm^{-2}. Research on TADF OLEDs culminated in 2012 after the work of Adachi and co-workers.[77] With the newly synthesized highly efficient TADF molecules, the EQE of the OLED device reached up to 30%, which clearly breaks the efficiency limit of fluorescent OLEDs and is comparable to those of rare metal-complex phosphorescent OLEDs. The emission colors of TADF materials have been shifted from blue to red, and the EQEs of OLED devices have reached 19.5% for blue and 30.0% for green TADF emitters, showing great potential for replacing the common noble metal-based complexes. These remarkable discoveries have truly revolutionized our understanding of organic semiconductors and optoelectronics. However, the already commercialized organic TADF emitters usually generated a broad emission spectrum (80–100 nm) arising from the vibronic coupling between the ground and excited states as well as the structural relaxation at excited states of organic emitters, which is detrimental to satisfying the requirement of high color purity displays based on R/G/B (red/green/blue) emitters.[5] Although the color purity of the original broad EL band can be modified by introducing a color filter and/or an optical microcavity in commercial OLED displays, this inevitably leads to a significant increase in cost and power consumption.[81,90] Thus, the development of efficient TADF emitters with narrowband emissions, especially those having the ability to achieve high

This journal is © The Royal Society of Chemistry 2022

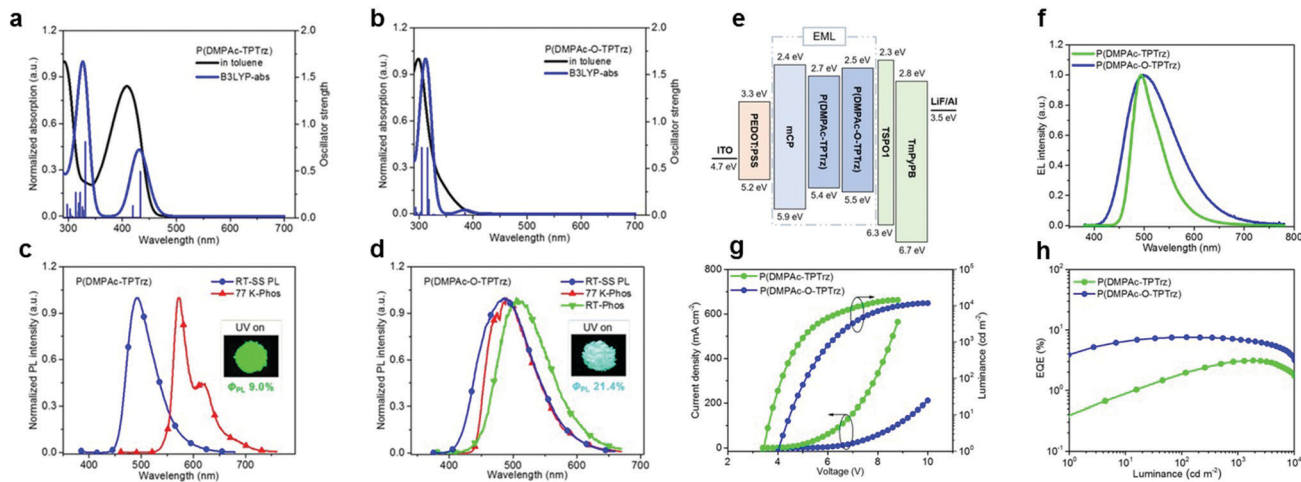J. Mater. Chem. C, 2022, **10**, 2333–2348 | **2339**

Fig. 7 Absorption spectra measured in toluene (black curve) and theoretical absorption spectra (blue curve) of P(DMPAc-TPTrz) (a) and P(DMPAc-O-TPTrz) (b). The steady-state PL spectra at room temperature, and phosphorescence spectra at 77 K and room temperature for the neat films of P(DMPAc-TPTrz) (c) and P(DMPAc-O-TPTrz) (d). Inset: Corresponding photos taken under a 365 nm UV lamp. (e) Device structure and related energy level diagram. (f) EL spectra. (g) Current−density−voltage−luminance characteristics. (h) EQE as a function of luminance. Reprinted with permission from ref. 88. Copyright 2020 John Wiley and Sons.

color purity that complies with the Commission Internationale de L'Eclairage (CIE) coordinates requirements defined by the broadcasting standards, is highly important.

In the past few years, TADF with MR effect induced HOMO–LUMO separation has shown great potential to deliver a narrow EL band.[91–94] For example, Hatakeyama et al. first reported two MR-TADF compounds with a B–N-containing core skeleton, which exhibited blue EL with a small FWHM of only 28 nm, a high maximum EQE$_{max}$ of 20.2%, and high color purity with CIE coordinates of (0.13, 0.09) which are close to the National Television System Committee (NTSC) blue light standard (CIE: (0.14, 0.08)).[95] The as-synthesized compounds with tert-butyl and carbazolyl units were subsequently modified and achieved blue OLEDs with a FWHM of only 27 nm, a high EQE$_{max}$ of 32.1%, and low efficiency roll-off.[96] Later, excellent electroluminescence performance with a high EQE of up to 34% and a narrowband emission with a FWHM of 14 nm was achieved for deep-blue OLEDs by incorporating a state-of-the-art MR-TADF emitter (ν-DABNA).[97] However, thus far, the available emission colors in MR-TADF have been restricted to the blue spectral region owing to the intrinsic difficulties associated with the bathochromic shifts of the MR-induced emissions while retaining TADF characteristics. Therefore, the realization of long wavelength or even full-color MR-TADF emitters with narrowband emissions for next-generation full color displays remains a great challenge. Green MR-TADF compounds exhibiting a narrow band (FWHM: 32–40 nm) with a high EQE$_{max}$ (20.9–22.7%) were reported, but the best CIE coordinates of (0.20, 0.58) largely deviated from the NTSC standard (CIE: (0.21, 0.71)).[98] To further redshift the emission to the green region, by precisely introducing an auxiliary donor group to the HOMO-distributed carbon atom of a MR skeleton, the resulting molecule was endowed with an emission beyond 520 nm and a narrow FWHM (Fig. 8a and b), exhibiting excellent color purity

(CIE: (0.23, 0.69)) and a high EQE$_{max}$ of 27%.[99] Intriguingly, an epoch-making strategy was reported for producing full-color, narrowband, and high-efficiency MR-TADF emitters by facile combinations of tricoordinate boron and carbazole moieties (Fig. 8c and f), achieving high EQE$_{max}$ values of 29.3%, 31.8%, and 22.0% for blue, green, and red, respectively.[100] However, due to the poor solubility and strong crystallization of organic molecules, OLEDs are generally fabricated by thermal evaporation which requires a high running cost, complicated device structures, and control preciseness to form multilayered device structures for enhancing the efficiency in injecting holes and electrons.[5,101] Comparatively, high-efficiency solution-processable emitting materials are indispensable.[102,103] A solution-processable MR-TADF material (OAB-ABP-1), with an fully resonating extended π-skeleton and bulky substituents, was designed, exhibiting a narrowband emission at 506 nm with a FWHM of 34 nm.[104] In addition, a solution-processed TADF-sensitized OLED with an EQE$_{max}$ of 3.8% with the emission spectrum centered at 840 nm and an emission FWHM below 40 nm was demonstrated.[105]

5. Prospects and challenges for RTP and TADF CQDs in displays

Benefiting from the abundant energy levels, the emerging quantum-confined CQDs have shown huge prospects in RTP and TADF for exploring the possibilities of implementing the next-generation displays.[106,107] In the last few years, steady efforts have been made to develop phosphorescent and delayed fluorescence CQDs through host–guest complexation strategies to prevent unnecessary triplet energy dissipation, in which isolated guest CQDs are homogeneously dispersed in hosts such as crystalline frameworks,[108] SiO$_2$,[109] boric acid[110] and inorganic crystalline nanocomposites.[111] However, this strategy
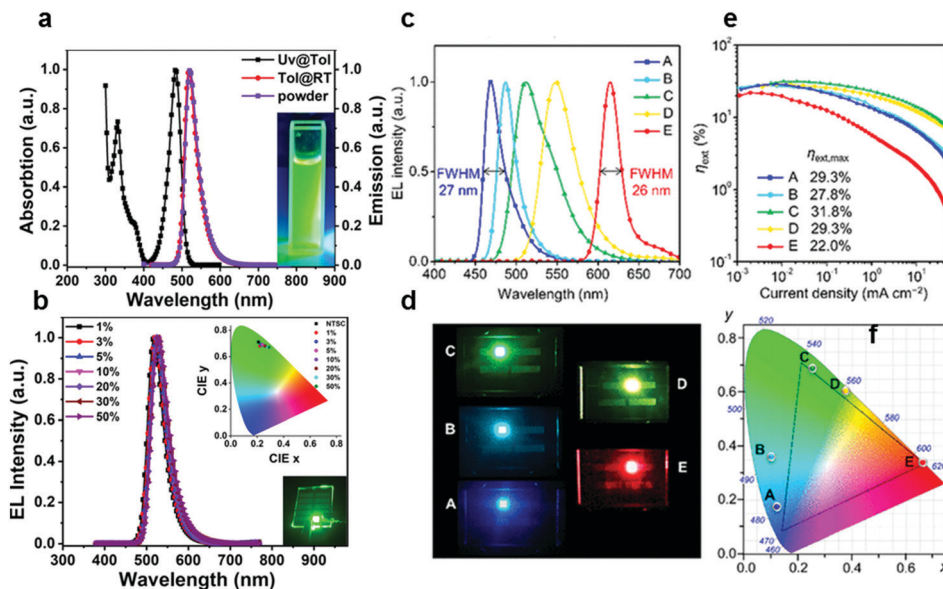
Fig. 8 (a) The normalized UV/Vis absorption and fluorescence spectra of m-Cz-BNCz measured in toluene solution and the corresponding powder fluorescence spectrum (inset: photograph in toluene taken under 365 nm UV light). (b) EL spectra of the devices (inset: the color coordinates of the devices and the photograph showing the emission color of the device at a 3 wt% doping concentration). Reprinted with permission from ref. 99. Copyright 2020 John Wiley and Sons; (c) EL characteristics of OLEDs (devices A–E) utilizing 1–5 as emitters. (d) EL spectra measured at 10 mA cm⁻². (e) Photographs showing full-color EL emissions (left) and their EL color coordinates (right). (f) η_{ext} versus current density plots. Reprinted with permission from ref. 100. Copyright 2020 American Chemical Society.

using CQD composites to achieve triplet-excited-state-involved emission is more vulnerable to phase segregation, poor thermal stability and conductivity, which severely impedes their practical applications,[112] and thus, undoubtedly, single-component CQDs with intrinsic RTP and TADF properties are highly desired. For example, a gram-scale method for the preparation of ultralong RTP CQDs (1.46 s)[113] and the hydrothermal treatment of levo-floxacin for synthesizing time-dependent phosphorescent CQDs exhibiting a change in phosphorescence color from orange to green and blue-green self-protective RTP emission based on fluorine and nitrogen codoped carbon dots[114] have been demonstrated, indicating the intrinsic ability of ISC in CQDs. Previously, we reported the first successful demonstration of single-component white emission derived from blue-yellow fluorescence–phosphorescence dual emission with an overall PLQY as high as 25% and a relatively high yellow phosphorescence with a Φ_P of 6% under ambient conditions based on W-CNQDs (Fig. 9a–e).[65] Experimental and theoretical investigations revealed that the key role of the carbonyl groups at the rim of W-CNQDs is in assisting the ISC arising from the carbonyl ($n\pi^\star$) mediated intermolecular ($\pi\pi^\star$) electronic coupling. In addition, some efforts have been made to explore CQD-based multicolor phosphorescence. For instance, a universal approach based on efficient radiative energy transfer was designed to obtain NIR-excited multicolor phosphorescent carbon dots.[115]

In contrast, studies about CQD-based TADF emitters are relatively rare due to their planar configurations.[116] Recently, a new design approach was reported to control ΔE_{ST} in graphene quantum dots/graphene oxide quantum dots by varying the ratio of oxygenated carbon to sp² carbon (γ_{OC}) (Fig. 9f–h).[117]

It was demonstrated that ΔE_{ST} decreases from 0.365 to 0.123 eV as γ_{OC} increases from 4.63% to 59.6%, which in turn induces a dramatic transition from RTP to TADF. Calculations based on time-dependent density functional theory elucidate that such behavior with the changing afterglow characteristics is attributed in part to the distorted molecular geometry and to the change of the SOC matrix element (SOCME) value with the increase of oxygen functional groups, providing a new approach to the engineering of ΔE_{ST} in GQDs for controlled realization of smart multimodal afterglow materials.

Despite the intensive work on CQD-based RTP and TADF emitters, the research of CQD-based triplet state modulation is still at an early stage with extremely low phosphorescence quantum efficiencies and long lifetimes (hundreds of milliseconds) compared with well-developed transition metal complexes. Furthermore, narrow-band (FWHM < 50 nm) and color-tunable RTP emissions are of great necessity and significance for the realization of a full-color electroluminescent display with high color purity. Therefore, the following problems need to be solved for applications in electroluminescence.

5.1 Chemical functionalization

The chemical functionalization of CQDs is a potential strategy to regulate their chemical, electronic, and photophysical properties.[118,119] Generally, CQDs prepared from either "top-down" or "bottom-up" synthetic approaches are indigenously functionalized with abundant surface groups, especially oxygen related functional groups, such as carboxyl and hydroxyl, which impart suitable chemically reactive groups for surface passivation and functionalization.[120] For instance, bandgap narrowing

This journal is © The Royal Society of Chemistry 2022

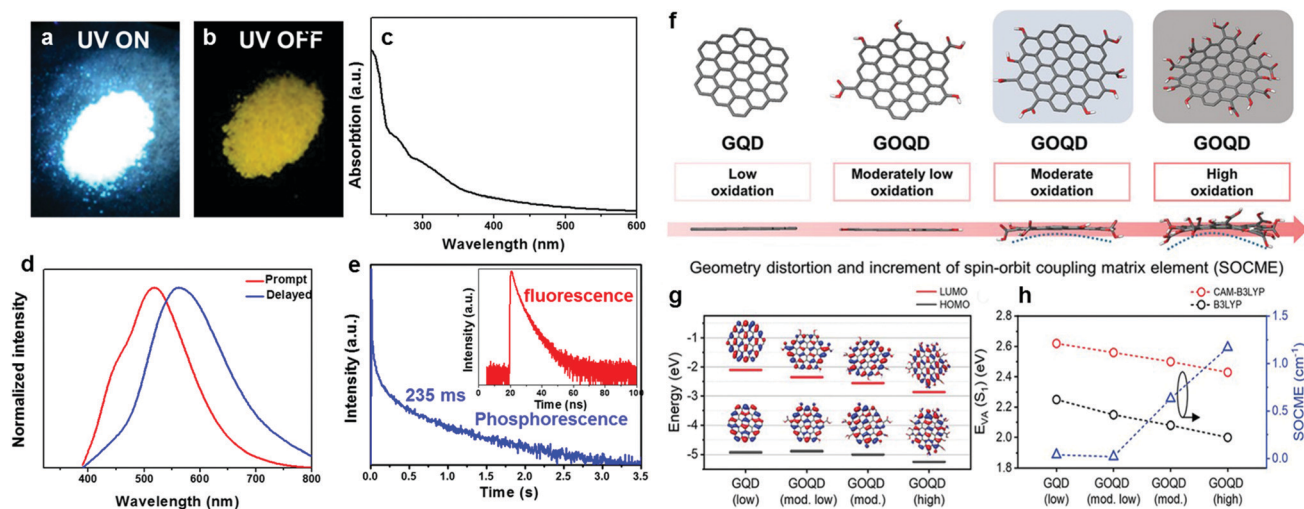J. Mater. Chem. C, 2022, 10, 2333–2348 | 2341

Fig. 9 Photographs taken before (a) and after (b) the UV light (365 nm) is turned off. (c) UV-vis absorption spectrum. (d) The prompt (red line) and delayed (blue line, 5 ms) PL spectra excited under 380 nm. (e) The time-resolved decay spectra measured at 520 nm for a long lifetime and at 440 nm for a short lifetime (inset) of W-CNQDs. Reprinted with permission from ref. 65. Copyright 2019 The Royal Society of Chemistry. (f) The optimized ground state calculated at the DFT level. (g) HOMO and LUMO for a series of GQDs at an optimized S_0. (h) Calculated vertical transition energies for the S_1 state at ground state geometry and SOCME values in accordance with the extent of oxidation. Reprinted with permission from ref. 117. Copyright 2020 John Wiley and Sons.

can be tailored by grafting GQDs with electron-donating/withdrawing functionalities.[121] Specifically, different polyaromatic compounds through the condensation reaction between $-COOH/-C=O$ and $-NH_2$ to form $N-C=O$ or $C=N$ amide bonds can be synthesized under solvothermal conditions. White-light-emitting GQDs through oxidative-cutting and post-synthesis functionalization with bulky Fréchet's dendritic wedges were synthesized,[122] which are soluble in common organic solvents, such as dichloromethane, tetrahydrofuran, and acetonitrile (Fig. 10a). Narrow emission (FWHM < 40 nm) was achieved through post-synthetic modifications of surface functional groups in which a boron-dipyrromethene dye was integrated into the carbon dots under solvothermal conditions (Fig. 10b–d).[123] The increased solubility of the large colloidal GQDs prepared from solution chemistry with a uniform and tunable size, e.g., samples 1–3, is achieved by multiple $2',4',6'$-trialkyl phenyl groups covalently attached to the edges of the graphene moieties.[124]

5.2 Efficient full-color phosphorescent and delayed fluorescence CQDs with short lifetimes

For next-generation electroluminescent displays, high-performance RTP and TADF CQDs with short lifetimes are highly demanded for breaking through the 5% limit of the traditional fluorescence devices. However, to date most of the reported triplet-excited-state-involved emissions of CQDs relying on host–guest systems generally exhibit dim luminescence because of inefficient SOC with lifetimes in the second regime[71,112] and, strictly speaking, persistent afterglow, which severely impede their practical applications. Accordingly, from a fundamental perspective, the most critical way to develop efficient CQD-based RTP or TADF emitters is to reduce ΔE_{ST} by manipulating the separation of the HOMO and the LUMO for boosting the ISC or RISC according to eqn (2) and (3). In fact,

CQDs possessing dominant (π, π^*) characteristic in singlet and triplet states normally have a large ΔE_{ST} due to their plane sp^2 π-conjugation domains and, consequently, a slow k_{ISC}. Following the design principle of pure organic RTP or TADF emitters using donor–acceptor systems, with CQDs regarded as either the donor or acceptor, after the incorporation of acceptor or donor sub-units, intramolecular charge-transfer states are generated, serving as intermediate states for minimizing ΔE_{ST}, and, thus, in theory, accelerating k_{ISC}. For instance, electron-donating aromatics, (donor) such as carbazole, diphenyl amine, phenoxazine, etc., can be grafted into CQDs containing electron-donating groups (acceptor) through one-pot reactions or post-synthetic modification for achieving efficient k_{ISC}. In addition, the RTP emission wavelengths of those CQDs were constrained to the blue or green region below 540 nm, and color-tunable RTP emissions are of great necessity and significance for full-color displays. On the basis of the enhancement of SOC based on $n-\pi$ transitions, by varying the π-conjugated units and edged functional group ratio in CQDs, the (n, π^*) and (π, π^*) molecular orbitals could be mixed to generate tunable T_1 state with distinct $^3(\pi, \pi^*)$ configuration and energy levels, which in turn enabled the tuning of phosphorescence color, lifetime, and quantum yield.[125]

Notably, when ΔE_{ST} is relatively small (<0.37 eV), a RISC process can occur, which may contribute to TADF emission.[86,99,117,126] Noteworthily, MR-TADF emitters with planar boron- and oxygen (or nitrogen)-containing arene compounds can be taken as an example for designing efficient CQD-based TADF emitters. Specifically, it is likely to select polycyclic aromatic hydrocarbons (PAHs) containing boron, nitrogen, phosphorus, and sulfur to prepare nanographenes, which is potentially advantageous for the production of complementary resonance effects of the electron density distributions on the HOMO and LUMO orbitals leading to a small ΔE_{ST} (Fig. 11).[127,128]

2342 | *J. Mater. Chem. C*, 2022, **10**, 2333–2348

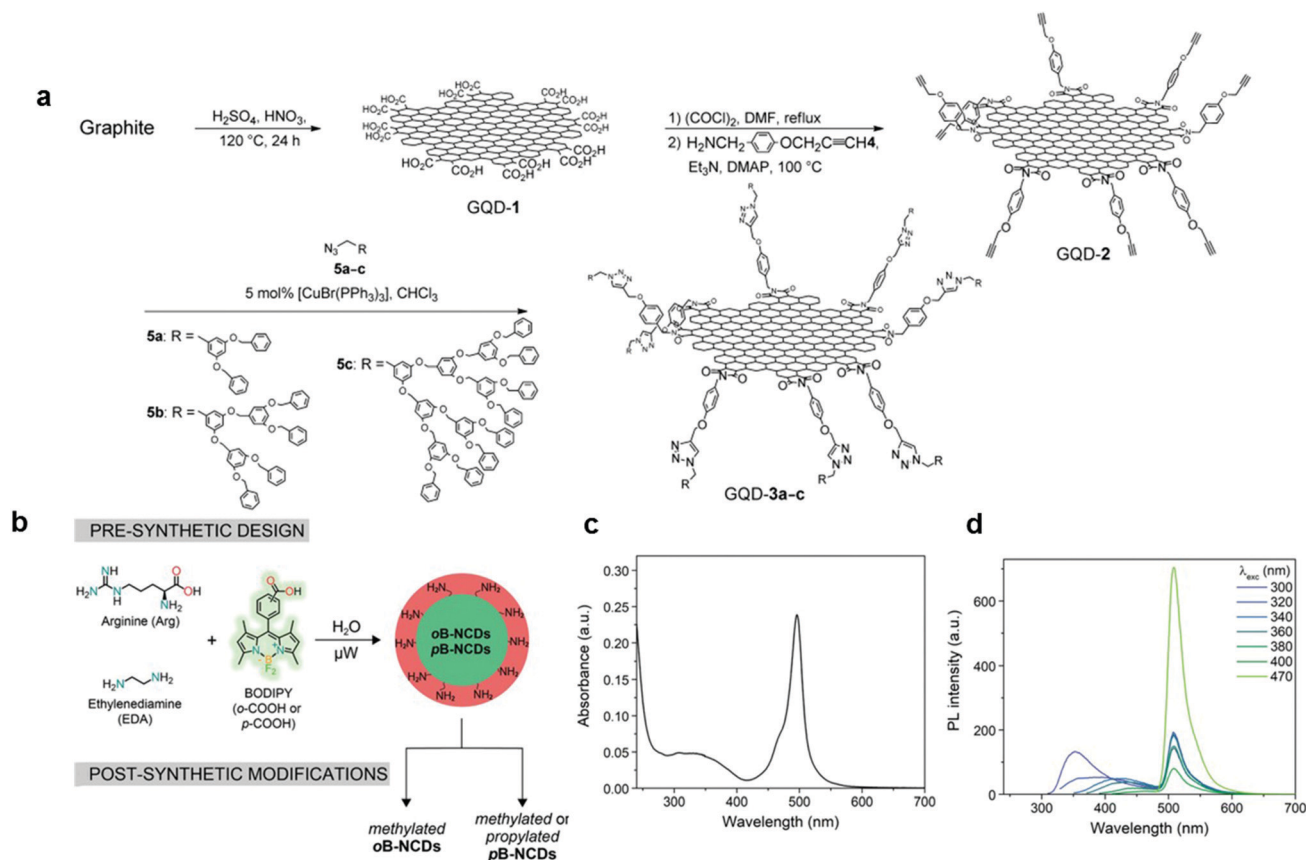This journal is © The Royal Society of Chemistry 2022

Fig. 10 (a) Preparation of GQD-2 and introduction of dendritic wedges by copper–catalyzed Huisgen cycloaddition. Reprinted with permission from ref. 122. Copyright 2014 John Wiley and Sons. (b) Precursors used for the synthesis of oB-NCDs and pB-NCDs and post-synthetic modification of the surface amino groups on the surface. (c) UV-Vis spectrum (5×10^{-2} mg mL^{-1}) and (d) PL emission spectra at different excitation wavelengths of pB-NCDs. Reprinted with permission from ref. 123. Copyright 2021 John Wiley and Sons.

5.3 Tailored design of CQDs for narrow emission

Narrowband emission is critically vital for achieving energy efficiency and a wide color gamut.[128–130] Some advances have been made in preparing narrow bandwidth CQDs ranging from blue to red with high PLQYs.[131–135] Particularly, the development of multicolored narrow bandwidth emission (FWHM of 30 nm) from triangular CQDs for high color-purity full-color LEDs opens up great prospects for the next-generation display technology.[41] Yet, the greatest challenges concern the rational synthesis of efficient phosphorescent and delayed fluorescence CQDs with a narrow bandwidth and their correspondingly intrinsic mechanism at the molecular level. Recently, a variety of B, N-PAHs such as DABNA-analogues have been developed as narrow bandwidth TADF emitters possessing planar and conjugate structures instead of the separation between donor and acceptor moieties for improved color purity (Fig. 12).[136] Therefore, a simple and versatile approach that enables the implementation of multiple boron centers and the modulation of their arrangement and electron-accepting nature is highly desirable to systematically investigate the structure–property relationship of nanographenes as actual functional π-conjugated materials. Choosing precursors with a B–N-containing skeleton to enlarge planar π-systems may become a feasible strategy for the development of novel CQD-based RTP or TADF emitters. For instance, triphenylboron, diphenylamine or triphenylamine combines neighboring phenyl groups to construct a rigid π-conjugated plane framework. Moreover, the nitrogen atom exhibits the opposite resonance effect of the boron atoms, and *para*-substitution relative to it can enhance the resonance effect and significantly separate the HOMO and LUMO without introducing donor or acceptor groups, resulting in a small ΔE_{ST}. Additionally, narrowband emissive CQDs can be developed using various modification agents, including small molecules and polymers.

5.4 Enhancing the organic solubility of CQDs

Solution processes, such as spin coating and ink-jet printing, show great potential in enabling low-cost and large-area manufacturability of QLEDs,[129,130] and hence good solubility of CQDs is indispensable for easily forming uniform thin films with low surface roughness. Undoubtedly, the good solution processability requirement increases the design difficulty of TADF emitters. On one hand, these molecules must have good enough solubility in common organic solvents to make a solution process feasible. On the other hand, these molecules

Fig. 11 The designed boron-doped and nitrogen-doped π-extended nanographene structures and oscillator strength, f_{osc}, as a function of ΔE_{ST} for 3–6. Reprinted with permission from ref. 128. Copyright 2020 John Wiley and Sons.

should form high quality and pinhole-free uniform films without aggregation and phase separation in the solution process. Furthermore, these films are expected to exhibit excellent morphological and thermal stabilities during device operation at high current densities.[137] Generally, CQDs prepared from "bottom-up" synthetic approaches are functionalized with abundant groups, such as carboxyl, amidogen and hydroxyl groups, indigenously endowing them with good solubility.[22] And the precursors chosen often determine the solubility of the resulting CQDs; alkyl precursors are ideal for the synthesis of CQDs. For example, the synthesis of three red-emitting electron-donating group passivated CQDs R-EGP-CQDs showing high solubility in *o*-dichlorobenzene (4.4–5.0 mg mL^{-1}) has been demonstrated.[31] Furthermore, the post-synthesis modification of CQDs is another potential strategy to regulate their solubility. The edge-functionalized GQD-2 and GQD-3a–c through the reaction of edge-oxidized GQDs with 4-propynyloxybenzylamine were synthesized,[122] endowing them with high solubility and good film-forming ability. By the introduction of *tert*-butyl substitution units into the molecular frameworks of NAI_R1, NAI_R2 and NAI_R3, the solubility in chlorobenzene was gradually enhanced as the number

of *tert*-butyl substitution units was increased from 17.5 to 200 mg mL^{-1}.[138,139] Intriguingly, a general edge chlorination protocol for atomically precise functionalization of nanographenes at different scales from 1.2 to 3.4 nm was presented, showing enhanced solution processability associated with decreases in the optical bandgap and frontier molecular orbital energy levels *via* the structure-correlated property modulation (Fig. 13).[139]
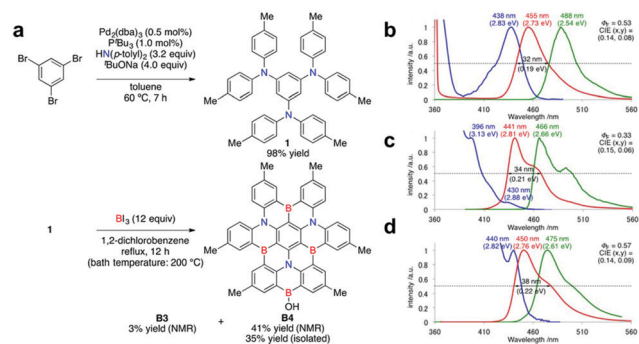

Fig. 12 (a) Two-step synthesis of B4. (b–d) Normalized absorption (blue), fluorescence (red), and phosphorescence (green, 77 K, 25 ms delay) spectra, with absorption/emission maxima, absolute fluorescence quantum yields (Φ_F), and FWHM of PMMA films of B2, B3, and B4 (1 wt%, excited at 360 nm). Reprinted with permission from ref. 136. Copyright 2018 American Chemical Society.
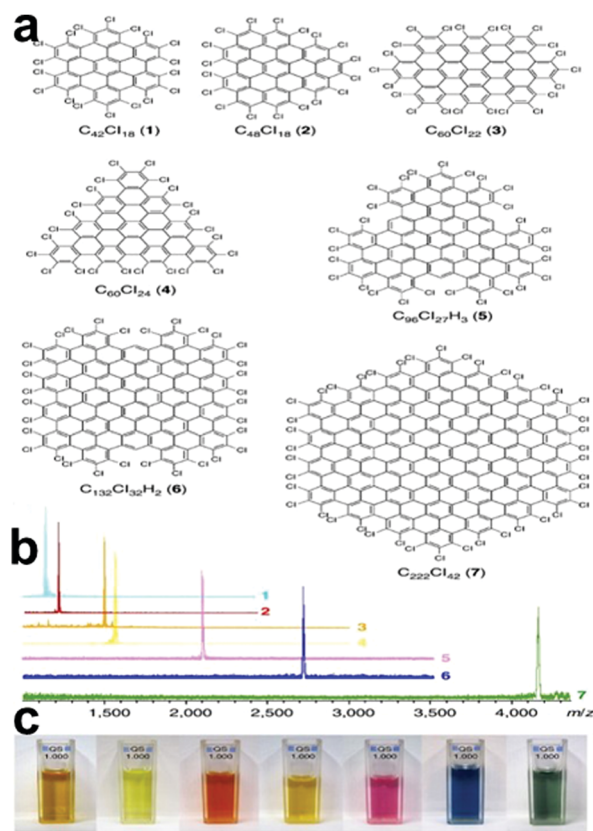

Fig. 13 Chlorinated nanographenes (1–7): (a) structural formulae; (b) mass spectra; and (c) photos of the toluene solutions of 1–7. Reprinted with permission from ref. 139. Copyright 2013 Springer.

2344 | *J. Mater. Chem. C*, 2022, **10**, 2333–2348

This journal is © The Royal Society of Chemistry 2022

Conflicts of interest

There are no conflicts to declare.

Acknowledgements

Notes and references

1 X. Wang, Z. Bao, Y.-C. Chang and R.-S. Liu, *ACS Energy Lett.*, 2020, **5**, 3374–3396.

2 Y. E. Panfil, M. Oded and U. Banin, *Angew. Chem., Int. Ed.*, 2018, **57**, 4274–4295.

3 J. Yang, M. K. Choi, U. J. Yang, S. Y. Kim, Y. S. Kim, J. H. Kim, D. H. Kim and T. Hyeon, *Nano Lett.*, 2021, **21**, 26–33.

4 J. Li, J. Chen, L. Xu, S. Liu, S. Lan, X. Li and J. Song, *Mater. Chem. Front.*, 2020, **4**, 1444–1453.

5 G. Hong, X. Gan, C. Leonhardt, Z. Zhang, J. Seibert, J. M. Busch and S. Brase, *Adv. Mater.*, 2021, **33**, 1–24.

6 A. Salehi, C. Dong, D. H. Shin, L. Zhu, C. Papa, A. Thy Bui, F. N. Castellano and F. So, *Nat. Commun.*, 2019, **10**, 2305.

7 C. Adachi, *Jpn. J. Appl. Phys.*, 2014, 53.

8 Y. Tao, K. Yuan, T. Chen, P. Xu, H. Li, R. Chen, C. Zheng, L. Zhang and W. Huang, *Adv. Mater.*, 2014, **26**, 7931–7958.

9 T.-L. Wu, M.-J. Huang, C.-C. Lin, P.-Y. Huang, T.-Y. Chou, R.-W. Chen-Cheng, H.-W. Lin, R.-S. Liu and C.-H. Cheng, *Nat. Photonics*, 2018, **12**, 235–240.

10 W. Zeng, H. Y. Lai, W. K. Lee, M. Jiao, Y. J. Shiu, C. Zhong, S. Gong, T. Zhou, G. Xie, M. Sarma, K. T. Wong, C. C. Wu and C. Yang, *Adv. Mater.*, 2018, **30**, 1704961.

11 K. Tuong, Ly, R.-W. Chen-Cheng, H.-W. Lin, Y.-J. Shiau, S.-H. Liu, P.-T. Chou, C.-S. Tsao, Y.-C. Huang and Y. Chi, *Nat. Photonics*, 2016, **11**, 63–68.

12 F. B. Dias, K. N. Bourdakos, V. Jankus, K. C. Moss, K. T. Kamtekar, V. Bhalla, J. Santos, M. R. Bryce and A. P. Monkman, *Adv. Mater.*, 2013, **25**, 3707–3714.

13 X. Dai, Z. Zhang, Y. Jin, Y. Niu, H. Cao, X. Liang, L. Chen, J. Wang and X. Peng, *Nature*, 2014, **515**, 96–99.

14 D. V. Talapin and J. Steckel, *MRS Bull.*, 2013, **38**, 685–691.

15 Y. Shu, X. Lin, H. Qin, Z. Hu, Y. Jin and X. Peng, *Angew. Chem., Int. Ed.*, 2020, **59**, 22312–22323.

16 X. Dai, Y. Deng, X. Peng and Y. Jin, *Adv. Mater.*, 2017, **29**, 1607022.

17 Y. H. Won, O. Cho, T. Kim, D. Y. Chung, T. Kim, H. Chung, H. Jang, J. Lee, D. Kim and E. Jang, *Nature*, 2019, **575**, 634–638.

18 H. Shen, Q. Gao, Y. Zhang, Y. Lin, Q. Lin, Z. Li, L. Chen, Z. Zeng, X. Li, Y. Jia, S. Wang, Z. Du, L. S. Li and Z. Zhang, *Nat. Photonics*, 2019, **13**, 192–197.

19 T. Kim, K. H. Kim, S. Kim, S. M. Choi, H. Jang, H. K. Seo, H. Lee, D. Y. Chung and E. Jang, *Nature*, 2020, **586**, 385–389.

20 T. Yuan, T. Meng, P. He, Y. Shi, Y. Li, X. Li, L. Fan and S. Yang, *J. Mater. Chem. C*, 2019, **7**, 6820–6835.

21 Y. Yan, J. Gong, J. Chen, Z. Zeng, W. Huang, K. Pu, J. Liu and P. Chen, *Adv. Mater.*, 2019, **31**, 1808283.

22 F. Yuan, S. Li, Z. Fan, X. Meng, L. Fan and S. Yang, *Nano Today*, 2016, **11**, 565–586.

23 A. Xu, G. Wang, Y. Li, H. Dong, S. Yang, P. He and G. Ding, *Small*, 2020, **16**, 2004621.

24 H. Ding, X.-X. Zhou, J.-S. Wei, X.-B. Li, B.-T. Qin, X.-B. Chen and H.-M. Xiong, *Carbon*, 2020, **167**, 322–344.

25 F. Yuan, Z. Wang, X. Li, Y. Li, Z. Tan, L. Fan and S. Yang, *Adv. Mater.*, 2017, **29**, 1–6.

26 T. Meng, Z. Wang, T. Yuan, X. Li, Y. Li, Y. Zhang and L. Fan, *Angew. Chem., Int. Ed.*, 2021, **60**, 16343–16348.

27 S. Li, W. Su, H. Wu, T. Yuan, C. Yuan, J. Liu, G. Deng, X. Gao, Z. Chen, Y. Bao, F. Yuan, S. Zhou, H. Tan, Y. Li, X. Li, L. Fan, J. Zhu, A. T. Chen, F. Liu, Y. Zhou, M. Li, X. Zhai and J. Zhou, *Nat. Biomed. Eng.*, 2020, **4**, 704–716.

28 H. Wu, H. Xu, Y. Shi, T. Yuan, T. Meng, Y. Zhang, W. Xie, X. Li, Y. Li and L. Fan, *Chin. J. Chem.*, 2021, **39**, 1364–1388.

29 W. Su, H. Wu, H. Xu, Y. Zhang, Y. Li, X. Li and L. Fan, *Mater. Chem. Front.*, 2020, **4**, 821–836.

30 W. Su, R. Guo, F. Yuan, Y. Li, X. Li, Y. Zhang, S. Zhou and L. Fan, *J. Phys. Chem. Lett.*, 2020, **11**, 1357–1363.

31 H. Jia, Z. Wang, T. Yuan, F. Yuan, X. Li, Y. Li, Z. Tan, L. Fan and S. Yang, *Adv. Sci.*, 2019, **6**, 1900397.

32 Z. Wang, F. Yuan, X. Li, Y. Li, H. Zhong, L. Fan and S. Yang, *Adv. Mater.*, 2017, **29**, 1702910.

33 T. Meng, T. Yuan, X. Li, Y. Li, L. Fan and S. Yang, *Chem. Commun.*, 2019, **55**, 6531–6534.

34 S. Zhu, Q. Meng, L. Wang, J. Zhang, Y. Song, H. Jin, K. Zhang, H. Sun, H. Wang and B. Yang, *Angew. Chem., Int. Ed.*, 2013, **52**, 4045–4049.

35 T. Feng, S. Tao, D. Yue, Q. Zeng, W. Chen and B. Yang, *Small*, 2020, **16**, 2001295.

36 Y. Han, B. Tang, L. Wang, H. Bao, Y. Lu, C. Guan, L. Zhang, M. Le, Z. Liu and M. Wu, *ACS Nano*, 2020, **14**, 14761–14768.

37 K. Jiang, S. Sun, L. Zhang, Y. Lu, A. Wu, C. Cai and H. Lin, *Angew. Chem., Int. Ed.*, 2015, **54**, 5360–5363.

38 L. Wang, W. Li, L. Yin, Y. Liu, H. Guo, J. Lai, Y. Han, G. Li, M. Li, J. Zhang, R. Vajtai, P. M. Ajayan and M. Wu, *Sci. Adv.*, 2020, **6**, eabb6772.

39 H. Ding, S. B. Yu, J. S. Wei and H. M. Xiong, *ACS Nano*, 2016, **10**, 484–491.

40 F. Yuan, Y.-K. Wang, G. Sharma, Y. Dong, X. Zheng, P. Li, A. Johnston, G. Bappi, J. Z. Fan, H. Kung, B. Chen, M. I. Saidaminov, K. Singh, O. Voznyy, O. M. Bakr, Z.-H. Lu and E. H. Sargent, *Nat. Photonics*, 2019, **14**, 171–176.

41 F. Yuan, T. Yuan, L. Sui, Z. Wang, Z. Xi, Y. Li, X. Li, L. Fan, Z. Tan, A. Chen, M. Jin and S. Yang, *Nat. Commun.*, 2018, **9**, 2249.

42 Z. Yang, Z. Mao, Z. Xie, Y. Zhang, S. Liu, J. Zhao, J. Xu, Z. Chi and M. P. Aldred, *Chem. Soc. Rev.*, 2017, **46**, 915–1016.

43 S. Xu, R. Chen, C. Zheng and W. Huang, *Adv. Mater.*, 2016, **28**, 9920–9940.

This journal is © The Royal Society of Chemistry 2022

J. Mater. Chem. C, 2022, **10**, 2333–2348 | **2345**

44 N. Gan, H. Shi, Z. An and W. Huang, *Adv. Funct. Mater.*, 2018, **28**, 1–24.

45 L. Xiao, Z. Chen, B. Qu, J. Luo, S. Kong, Q. Gong and J. Kido, *Adv. Mater.*, 2011, **23**, 926–952.

46 M. Y. Wong and E. Zysman-Colman, *Adv. Mater.*, 2017, **29**, 1605444.

47 W. Zhao, T. S. Cheung, N. Jiang, W. Huang, J. W. Y. Lam, X. Zhang, Z. He and B. Z. Tang, *Nat. Commun.*, 2019, **10**, 1595.

48 J. Wang, X. Gu, H. Ma, Q. Peng, X. Huang, X. Zheng, S. H. P. Sung, G. Shan, J. W. Y. Lam, Z. Shuai and B. Z. Tang, *Nat. Commun.*, 2018, **9**, 2963.

49 O. Bolton, K. Lee, H. J. Kim, K. Y. Lin and J. Kim, *Nat. Chem.*, 2011, **3**, 205–210.

50 Z. An, C. Zheng, Y. Tao, R. Chen, H. Shi, T. Chen, Z. Wang, H. Li, R. Deng, X. Liu and W. Huang, *Nat. Mater.*, 2015, **14**, 685–690.

51 Z. Yang, Z. Mao, X. Zhang, D. Ou, Y. Mu, Y. Zhang, C. Zhao, S. Liu, Z. Chi, J. Xu, Y. C. Wu, P. Y. Lu, A. Lien and M. R. Bryce, *Angew. Chem., Int. Ed.*, 2016, **55**, 2181–2185.

52 Z. He, W. Zhao, J. W. Y. Lam, Q. Peng, H. Ma, G. Liang, Z. Shuai and B. Z. Tang, *Nat. Commun.*, 2017, **8**, 416.

53 S. Xu, W. Wang, H. Li, J. Zhang, R. Chen, S. Wang, C. Zheng, G. Xing, C. Song and W. Huang, *Nat. Commun.*, 2020, **11**, 4802.

54 Z. Xie, X. Zhang, H. Wang, C. Huang, H. Sun, M. Dong, L. Ji, Z. An, T. Yu and W. Huang, *Nat. Commun.*, 2021, **12**, 3522.

55 X. Zhang, L. Du, W. Zhao, Z. Zhao, Y. Xiong, X. He, P. F. Gao, P. Alam, C. Wang, Z. Li, J. Leng, J. Liu, C. Zhou, J. W. Y. Lam, D. L. Phillips, G. Zhang and B. Z. Tang, *Nat. Commun.*, 2019, **10**, 5161.

56 C. Chen, Z. Chi, K. C. Chong, A. S. Batsanov, Z. Yang, Z. Mao, Z. Yang and B. Liu, *Nat. Mater.*, 2021, **20**, 175–180.

57 J. Yang, Z. Ren, Z. Xie, Y. Liu, C. Wang, Y. Xie, Q. Peng, B. Xu, W. Tian, F. Zhang, Z. Chi, Q. Li and Z. Li, *Angew. Chem., Int. Ed.*, 2017, **56**, 880–884.

58 H. Wang, H. Shi, W. Ye, X. Yao, Q. Wang, C. Dong, W. Jia, H. Ma, S. Cai, K. Huang, L. Fu, Y. Zhang, J. Zhi, L. Gu, Y. Zhao, Z. An and W. Huang, *Angew. Chem., Int. Ed.*, 2019, **58**, 18776–18782.

59 L. Gu, H. Shi, L. Bian, M. Gu, K. Ling, X. Wang, H. Ma, S. Cai, W. Ning, L. Fu, H. Wang, S. Wang, Y. Gao, W. Yao, F. Huo, Y. Tao, Z. An, X. Liu and W. Huang, *Nat. Photonics*, 2019, **13**, 406–411.

60 J. Yang, X. Zhen, B. Wang, X. Gao, Z. Ren, J. Wang, Y. Xie, J. Li, Q. Peng, K. Pu and Z. Li, *Nat. Commun.*, 2018, **9**, 840.

61 P. Alam, N. L. C. Leung, J. Liu, T. S. Cheung, X. Zhang, Z. He, R. T. K. Kwok, J. W. Y. Lam, H. H. Y. Sung, I. D. Williams, C. C. S. Chan, K. S. Wong, Q. Peng and B. Z. Tang, *Adv. Mater.*, 2020, **32**, 2001026.

62 K. Jiang, X. Gao, X. Feng, Y. Wang, Z. Li and H. Lin, *Angew. Chem., Int. Ed.*, 2020, **59**, 1263–1269.

63 Y. Deng, D. Zhao, X. Chen, F. Wang, H. Song and D. Shen, *Chem. Commun.*, 2013, **49**, 5751–5753.

64 S. Tao, S. Lu, Y. Geng, S. Zhu, S. A. T. Redfern, Y. Song, T. Feng, W. Xu and B. Yang, *Angew. Chem., Int. Ed.*, 2018, **57**, 2393–2398.

65 T. Yuan, F. Yuan, X. Li, Y. Li, L. Fan and S. Yang, *Chem. Sci.*, 2019, **10**, 9801–9806.

66 J. Zhu, X. Bai, X. Chen, H. Shao, Y. Zhai, G. Pan, H. Zhang, E. V. Ushakova, Y. Zhang, H. Song and A. L. Rogach, *Adv. Opt. Mater.*, 2019, 1801599.

67 Kenry, C. Chen and B. Liu, *Nat. Commun.*, 2019, **10**, 1–15.

68 W. Zhao, Z. He and B. Z. Tang, *Nat. Rev. Mater.*, 2020, **5**, 869–885.

69 W. Zhao, Z. He, J. W. Y. Lam, Q. Peng, H. Ma, Z. Shuai, G. Bai, J. Hao and B. Z. Tang, *Chem*, 2016, **1**, 592–602.

70 T. Zhang, X. Ma, H. Wu, L. Zhu, Y. Zhao and H. Tian, *Angew. Chem., Int. Ed.*, 2020, **59**, 11206–11216.

71 H. Zhang, B. Wang, X. Yu, J. Li, J. Shang and J. Yu, *Angew. Chem., Int. Ed.*, 2020, **59**, 19390–19402.

72 S. Tao, S. Zhu, T. Feng, C. Zheng and B. Yang, *Angew. Chem., Int. Ed.*, 2020, **59**, 9826–9840.

73 G. Baryshnikov, B. Minaev and H. Agren, *Chem. Rev.*, 2017, **117**, 6500–6537.

74 Q. Peng, H. Ma and Z. Shuai, *Acc. Chem. Res.*, 2021, **54**, 940–949.

75 Y. Xiong, Z. Zhao, W. Zhao, H. Ma, Q. Peng, Z. He, X. Zhang, Y. Chen, X. He, J. W. Y. Lam and B. Z. Tang, *Angew. Chem., Int. Ed.*, 2018, **57**, 7997–8001.

76 R. Ishimatsu, S. Matsunami, K. Shizu, C. Adachi, K. Nakano and T. Imato, *J. Phys. Chem. A*, 2013, **117**, 5607–5612.

77 H. Uoyama, K. Goushi, K. Shizu, H. Nomura and C. Adachi, *Nature*, 2012, **492**, 234–238.

78 S. Hirata, Y. Sakai, K. Masui, H. Tanaka, S. Y. Lee, H. Nomura, N. Nakamura, M. Yasumatsu, H. Nakanotani, Q. Zhang, K. Shizu, H. Miyazaki and C. Adachi, *Nat. Mater.*, 2015, **14**, 330–336.

79 D. H. Ahn, S. W. Kim, H. Lee, I. J. Ko, D. Karthik, J. Y. Lee and J. H. Kwon, *Nat. Photonics*, 2019, **13**, 540–546.

80 Q. Zhang, B. Li, S. Huang, H. Nomura, H. Tanaka and C. Adachi, *Nat. Photonics*, 2014, **8**, 326–332.

81 J.-M. Teng, Y.-F. Wang and C.-F. Chen, *J. Mater. Chem. C*, 2020, **8**, 11340–11353.

82 E. Hamzehpoor and D. F. Perepichka, *Angew. Chem., Int. Ed.*, 2020, **59**, 9977–9981.

83 H. Ma, Q. Peng, Z. An, W. Huang and Z. Shuai, *J. Am. Chem. Soc.*, 2019, **141**, 1010–1015.

84 Y. Shoji, Y. Ikabata, Q. Wang, D. Nemoto, A. Sakamoto, N. Tanaka, J. Seino, H. Nakai and T. Fukushima, *J. Am. Chem. Soc.*, 2017, **139**, 2728–2733.

85 S. Wang, X. Yan, Z. Cheng, H. Zhang, Y. Liu and Y. Wang, *Angew. Chem., Int. Ed.*, 2015, **54**, 13068–13072.

86 M. Yang, S. Shikita, H. Min, I. S. Park, H. Shibata, N. Amanokura and T. Yasuda, *Angew. Chem., Int. Ed.*, 2021, **60**, 1–7.

87 R. Kabe, N. Notsuka, K. Yoshida and C. Adachi, *Adv. Mater.*, 2016, **28**, 655–660.

88 X. Liu, L. Yang, X. Li, L. Zhao, S. Wang, Z. H. Lu, J. Ding and L. Wang, *Angew. Chem., Int. Ed.*, 2021, **60**, 2455–2463.

89 A. Endo, M. Ogasawara, A. Takahashi, D. Yokoyama, Y. Kato and C. Adachi, *Adv. Mater.*, 2009, **21**, 4802–4806.

90 J. M. Ha, S. H. Hur, A. Pathak, J.-E. Jeong and H. Y. Woo, *NPG Asia Mater.*, 2021, **13**, 53.

91 S. Oda, W. Kumano, T. Hama, R. Kawasumi, K. Yoshiura and T. Hatakeyama, *Angew. Chem., Int. Ed.*, 2021, **60**, 2882–2886.

92 H. Zhang, G. Li, X. Guo, K. Zhang, B. Zhang, X. Guo, Y. Li, J. Fan, Z. Wang, D. Ma and B. Z. Tang, *Angew. Chem., Int. Ed.*, 2021, **60**, 22241–22247.

93 H. Tanaka, S. Oda, G. Ricci, H. Gotoh, K. Tabata, R. Kawasumi, D. Beljonne, Y. Olivier and T. Hatakeyama, *Angew. Chem., Int. Ed.*, 2021, **60**, 17910–17914.

94 M. Nagata, H. Min, E. Watanabe, H. Fukumoto, Y. Mizuhata, N. Tokitoh, T. Agou and T. Yasuda, *Angew. Chem., Int. Ed.*, 2021, 1–7.

95 T. Hatakeyama, K. Shiren, K. Nakajima, S. Nomura, S. Nakatsuka, K. Kinoshita, J. Ni, Y. Ono and T. Ikuta, *Adv. Mater.*, 2016, **28**, 2777–2781.

96 X. Liang, Z. P. Yan, H. B. Han, Z. G. Wu, Y. X. Zheng, H. Meng, J. L. Zuo and W. Huang, *Angew. Chem., Int. Ed.*, 2018, **57**, 11316–11320.

97 Y. Kondo, K. Yoshiura, S. Kitera, H. Nishi, S. Oda, H. Gotoh, Y. Sasada, M. Yanai and T. Hatakeyama, *Nat. Photonics*, 2019, **13**, 678–682.

98 Y. Zhang, D. Zhang, J. Wei, Z. Liu, Y. Lu and L. Duan, *Angew. Chem., Int. Ed.*, 2019, **58**, 16912–16917.

99 Y. Xu, C. Li, Z. Li, Q. Wang, X. Cai, J. Wei and Y. Wang, *Angew. Chem., Int. Ed.*, 2020, **59**, 17442–17446.

100 M. Yang, I. S. Park and T. Yasuda, *J. Am. Chem. Soc.*, 2020, **142**, 19468–19472.

101 S. O. Jeon, K. H. Lee, J. S. Kim, S.-G. Ihn, Y. S. Chung, J. W. Kim, H. Lee, S. Kim, H. Choi and J. Y. Lee, *Nat. Photonics*, 2021, **15**, 208–215.

102 S. Y. Lee, T. Yasuda, H. Komiyama, J. Lee and C. Adachi, *Adv. Mater.*, 2016, **28**, 4019–4024.

103 T. Huang, W. Jiang and L. Duan, *J. Mater. Chem. C*, 2018, **6**, 5577–5596.

104 N. Ikeda, S. Oda, R. Matsumoto, M. Yoshioka, D. Fukushima, K. Yoshiura, N. Yasuda and T. Hatakeyama, *Adv. Mater.*, 2020, **32**, 2004072.

105 A. Shahalizad, A. Malinge, L. Hu, G. Laflamme, L. Haeberlé, D. M. Myers, J. Mao, W. G. Skene and S. Kéna-Cohen, *Adv. Funct. Mater.*, 2020, **31**, 2007119.

106 G. Ragazzon, A. Cadranel, E. V. Ushakova, Y. Wang, D. M. Guldi, A. L. Rogach, N. A. Kotov and M. Prato, *Chem*, 2021, **7**, 606–628.

107 M. Semeniuk, Z. Yi, V. Poursorkhabi, J. Tjong, S. Jaffer, Z. H. Lu and M. Sain, *ACS Nano*, 2019, **13**, 6224–6255.

108 B. Wang, Y. Yu, H. Zhang, Y. Xuan, G. Chen, W. Ma, J. Li and J. Yu, *Angew. Chem., Int. Ed.*, 2019, **58**, 18443–18448.

109 Y. Sun, S. Liu, L. Sun, S. Wu, G. Hu, X. Pang, A. T. Smith, C. Hu, S. Zeng, W. Wang, Y. Liu and M. Zheng, *Nat. Commun.*, 2020, **11**, 559.

110 W. Li, W. Zhou, Z. Zhou, H. Zhang, X. Zhang, J. Zhuang, Y. Liu, B. Lei and C. Hu, *Angew. Chem., Int. Ed.*, 2019, **58**, 7278–7283.

111 D. C. Green, M. A. Holden, M. A. Levenstein, S. Zhang, B. R. G. Johnson, J. Gala de Pablo, A. Ward, S. W. Botchway and F. C. Meldrum, *Nat. Commun.*, 2019, **10**, 206.

112 Y. Sun, X. Zhang, J. Zhuang, H. Zhang, C. Hu, M. Zheng, B. Lei and Y. Liu, *Carbon*, 2020, **165**, 306–316.

113 K. Jiang, Y. Wang, X. Gao, C. Cai and H. Lin, *Angew. Chem., Int. Ed.*, 2018, **57**, 6216–6220.

114 P. Long, Y. Feng, C. Cao, Y. Li, J. Han, S. Li, C. Peng, Z. Li and W. Feng, *Adv. Funct. Mater.*, 2018, 1800791.

115 Y. Zheng, H. Wei, P. Liang, X. Xu, X. Zhang, H. Li, C. Zhang, C. Hu, X. Zhang, B. Lei, W. Y. Wong, Y. Liu and J. Zhuang, *Angew. Chem., Int. Ed.*, 2021, **60**, 22253–22259.

116 J. Liu, N. Wang, Y. Yu, Y. Yan, H. Zhang, J. Li and J. Yu, *Sci. Adv.*, 2017, e1603171.

117 M. Park, H. S. Kim, H. Yoon, J. Kim, S. Lee, S. Yoo and S. Jeon, *Adv. Mater.*, 2020, **32**, 1–10.

118 R. Cheng, Y. Xiang, R. Guo, L. Li, G. Zou, C. Fu, H. Hou and X. Ji, *Small*, 2021, 2102091.

119 X. Miao, D. Qu, D. Yang, B. Nie, Y. Zhao, H. Fan and Z. Sun, *Adv. Mater.*, 2018, **30**, 1704740.

120 C. Hu, M. Li, J. Qiu and Y. P. Sun, *Chem. Soc. Rev.*, 2019, **48**, 2315–2337.

121 Y. Yan, J. Chen, N. Li, J. Tian, K. Li, J. Jiang, J. Liu, Q. Tian and P. Chen, *ACS Nano*, 2018, **12**, 3523–3532.

122 R. Sekiya, Y. Uemura, H. Murakami and T. Haino, *Angew. Chem., Int. Ed.*, 2014, **53**, 5619–5623.

123 F. Arcudi, L. Ethordevic, S. Rebeccani, M. Cacioppo, A. Zanut, G. Valenti, F. Paolucci and M. Prato, *Adv. Sci.*, 2021, **8**, 2100125.

124 X. Yan, X. Cui and L.-S. Li, *J. Am. Chem. Soc.*, 2010, **132**, 5944–5945.

125 W. Ye, H. Ma, H. Shi, H. Wang, A. Lv, L. Bian, M. Zhang, C. Ma, K. Ling, M. Gu, Y. Mao, X. Yao, C. Gao, K. Shen, W. Jia, J. Zhi, S. Cai, Z. Song, J. Li, Y. Zhang, S. Lu, K. Liu, C. Dong, Q. Wang, Y. Zhou, W. Yao, Y. Zhang, H. Zhang, Z. Zhang, X. Hang, Z. An, X. Liu and W. Huang, *Nat. Mater.*, 2021, **9**, 1–7.

126 C.-Y. Chan, M. Tanaka, Y.-T. Lee, Y.-W. Wong, H. Nakanotani, T. Hatakeyama and C. Adachi, *Nat. Photonics*, 2021, **15**, 203–207.

127 A. Pershin, D. Hall, V. Lemaur, J. C. Sancho-Garcia, L. Muccioli, E. Zysman-Colman, D. Beljonne and Y. Olivier, *Nat. Commun.*, 2019, **10**, 597.

128 S. Madayanad Suresh, D. Hall, D. Beljonne, Y. Olivier and E. Zysman-Colman, *Adv. Funct. Mater.*, 2020, **30**, 1908677.

129 Y. Shirasaki, G. J. Supran, M. G. Bawendi and V. Bulović, *Nat. Photonics*, 2012, **7**, 13–23.

130 D. Zhang, T. Huang and L. Duan, *Adv. Mater.*, 2020, **32**, 1902391.

131 J. Liu, Y. Geng, D. Li, H. Yao, Z. Huo, Y. Li, K. Zhang, S. Zhu, H. Wei, W. Xu, J. Jiang and B. Yang, *Adv. Mater.*, 2020, **32**, 1906641.

132 L. Pan, S. Sun, L. Zhang, K. Jiang and H. Lin, *Nanoscale*, 2016, **8**, 17350–17356.

133 F. Yuan, P. He, Z. Xi, X. Li, Y. Li, H. Zhong, L. Fan and S. Yang, *Nano Res.*, 2019, **12**, 1669–1674.

134 Y. Liu, H. Gou, X. Huang, G. Zhang, K. Xi and X. Jia, *Nanoscale*, 2020, **12**, 1589–1601.

135 Z. Han, Y. Ni, J. Ren, W. Zhang, Y. Wang, Z. Xie, S. Zhou and S. F. Yu, *Nanoscale*, 2019, **11**, 11577–11583.

This journal is © The Royal Society of Chemistry 2022

J. Mater. Chem. C, 2022, **10**, 2333–2348 | **2347**

136 K. Matsui, S. Oda, K. Yoshiura, K. Nakajima, N. Yasuda and T. Hatakeyama, *J. Am. Chem. Soc.*, 2018, **140**, 1195–1198.

137 Y. Zhang, J. Wu, J. Song, Z. Chen, J. He, X. Wang, H. Liu, S. Chen, J. Qu and W.-Y. Wong, *Adv. Electron. Mater.*, 2019, **5**, 1800677.

138 W. Zeng, T. Zhou, W. Ning, C. Zhong, J. He, S. Gong, G. Xie and C. Yang, *Adv. Mater.*, 2019, **31**, 1901404.

139 Y. Z. Tan, B. Yang, K. Parvez, A. Narita, S. Osella, D. Beljonne, X. Feng and K. Mullen, *Nat. Commun.*, 2013, **4**, 2646.

2348 | *J. Mater. Chem. C*, 2022, **10**, 2333–2348

This journal is © The Royal Society of Chemistry 2022